Journal of Catalysis **207,** 57–65 (2002)
doi:10.1006/jcat.2002.3531, available online at http://www.idealibrary.com on IDEAL®

Characterisation of Supported Chromium Oxide Catalysts by Kinetic Analysis of H_2-TPR Data

Jaana M. Kanervo[1] and A. Outi I. Krause

Department of Chemical Technology, Helsinki University of Technology, P.O. Box 6100, FIN-02015 Hut, Finland

Received September 28, 2001; revised December 21, 2001; accepted December 28, 2001

The kinetics of reduction of chromium oxide catalysts was studied by applying nonlinear regression analysis to the temperature-programmed reduction (TPR) data of six different CrO_x/Al_2O_3 samples (1.2–14 wt% Cr). Different kinetic models were tested. Three heating rates were required to discriminate between the different kinetic models. The best-fit kinetic models and the estimated parameters for each sample are reported. The two-dimensional nuclei growth model suitably described the kinetics of reduction of samples with loading close to or beyond the monolayer content (>5 wt%). The overall reduction mechanism seemed to be the same irrespective of the method of catalyst preparation. The chromium content was important, however. Reducibility increased regularly with chromium loading, supporting the idea of a topochemical reduction mechanism. The sample with low chromium content (∼1 wt%) was reduced by a different overall mechanism than were the other samples and its reduction behaviour was best described by homogeneous first-order kinetics (random nucleation). Complete line-shape analysis of TPR patterns offers a good means for quantitative characterisation of alumina-supported chromium oxide catalysts, since it provides information on dynamic redox behaviour of the active sites.

Key Words: **supported chromium oxide; kinetics of reduction; TPR.**

INTRODUCTION

Supported chromium oxides are industrially important catalytic materials. They are used in polymerisation, dehydrogenation–hydrogenation, oxidation, isomerisation, aromatisation, and deNO_x reactions (1). Given the wide application of chromium oxide catalysts, it is not surprising that they have been exhaustively studied and continue to attract attention. Recent studies on supported chromium oxides for dehydrogenation focus on the identification of active sites, the influence of preparation and pretreatments on chromium oxide species formation, catalytic activity and selectivity, and the dehydrogenation mechanism (1). Characterisation of the molecular structure of supported chromium species offers a considerable challenge, since deposition of this metal ion on support may result in (i) isolated chromium ions, (ii) a two-dimensional chromium oxide overlayer, or (iii) three-dimensional chromium oxide crystallites (1). There are also various possible molecular structures for each phase (1).

One of the numerous methods used to characterise chromium oxide catalysts is temperature-programmed reduction (TPR) (2–4). Conventionally, TPR investigations have focused on studying the interaction between the chromium oxide and the catalyst support, comparing different preparation and pretreatment methods and material parameters. Although it is usually disregarded TPR patterns also contain kinetic information. The TPR technique for characterisation of solid material and kinetic modelling has been described and reviewed since the early 1980s (5–10). Ehrhardt *et al.* (2) have suggested a mathematical model for analysing complex nonisothermal reduction processes and demonstrated it for the H_2-reduction of CrO_3/SiO_2 (<1.0 wt% Cr). The kinetic model they proposed included three chromium species of different reducibility. Kinetics of CO reduction of supported chromium oxide has been studied under isothermal conditions by Dekker *et al.* (11) and Bensalem *et al.* (12). Dekker *et al.* (11) carried out concentration step response experiments with samples containing 10 wt% Cr_2O_3 on Al_2O_3 and transient kinetic modelling. They assumed the Langmuir–Hinshelwood mechanism for the reduction and estimated rate constants for CO adsorption and surface reaction, the maximum number of removable oxygen, the initial fraction of free sites, and the oxygen coordination number. Bensalem *et al.* (12) introduced *in situ* UV–visible (UV–vis)–near IR spectroscopy to directly monitor the reduction degree of samples containing 0.1–1.2 wt% Cr. They conducted kinetic modelling of reduction reactions and estimated rate constants for CO adsorption and desorption and the surface reduction reaction.

The reduction of chromium is significant for dehydrogenation since the catalysts are activated for dehydrogenation reaction by reduction. The dehydrogenation reaction presumably involves Cr^{3+} as an active site (1, 16). Our present study was carried out to increase understanding of the reduction of a supported chromium oxide catalyst through kinetic modelling of H_2-TPR data. In a previous

[1] To whom correspondence should be addressed. Fax: +358 9 451 2622. E-mail: kanervo@polte.hut.fi.

0021-9517/02 $35.00

study of the reduction kinetics of a monolayer CrO_x/Al_2O_3 catalyst (13), we found that the overall reduction of the catalyst could best be described by a two-dimensional nuclei growth model (Avrami–Erofeyev). We now undertake comparative investigations on a series of samples with different chromium loadings (1.2–13.5 wt%) prepared by the atomic layer deposition (ALD) technique and on a commercial chromia catalyst intended for fluidised bed operation. The ALD series was earlier investigated for dehydrogenation of butanes, by Hakuli and coworkers (14, 16, 18, 25) and Kytökivi *et al*. (15). Thus information is available on the preparation, characterisation, and activity measurements of catalysts similar to those studied here. In this work, TPR data was investigated by applying the conventional Kissinger method (21) and the Friedman method (22). In addition, nonlinear regression analysis was introduced. In this methodology gas–solid reaction models were tested against the experimental data by model fitting. These TPR kinetic results are discussed in terms of topochemical hypotheses, and the kinetic behaviour of reduction is correlated with other catalyst characterisation information. The Kissinger and the Friedman results were included in this work to demonstrate that they give results that deviate from those of our primary methodology.

EXPERIMENTAL

Catalysts

The catalysts were prepared by atomic layer deposition (ALD), a technique used for preparing highly dispersed supported catalysts. The reactive adsorption step, involving saturating gas–solid reactions between chromium acetyl acetonate $Cr(acac)_3$ and the pretreated support (γ-Al_2O_3, Akzo Nobel 000-1.5E) at 200°C, was followed by air treatment (600°C, 3–4 h) to remove the ligand residues. To obtain different chromium loadings (1.2–13.5%) these two-step cycles were performed 1 to 12 times. The ALD catalysts examined are labelled ALD1–ALD5. More detailed information on the catalyst preparation can be found elsewhere (14–16). A commercial CrO_x/Al_2O_3 fluidised bed catalyst (FB) was included in the study to allow comparison of the reduction mechanisms.

After preparation, the CrO_x/Al_2O_3 catalysts contained chromium in oxidation states Cr^{6+} and Cr^{3+} (X-ray photoelectron spectroscopy (XPS); experimental details can be found in Ref. (15)). Total chromium contents were determined by instrumental neutron activation analysis for samples ALD2–ALD4, and by atomic absorption spectroscopy (AAS) for samples ALD1 and ALD5. UV–vis spectrophotometry was applied to determine the amount of hexavalent chromium (Cr^{+6}) on the calcined ALD samples (17). No crystalline chromia phases on the ALD catalysts were detected in X-ray diffraction analysis. Table 1 summarises the preparation of the catalyst samples and their total chromium contents and the Cr^{6+} concentrations of the calcined samples.

TABLE 1

Description of Catalyst Samples

Sample	Number of ALD cycles	Total chromium content (wt%)	Cr^{6+} content (wt%)	AOS[a]	Particle size (mm)
ALD1	1	1.2	0.9	+2.6	0.2–0.4
ALD2	4	4.7	2.4	+2.7	0.7–1.0
ALD3	6	7.5	2.9	+2.9	0.7–1.0
ALD4	10	11.9	3.0	+2.8	0.7–1.0
ALD5	12	13.5	3.1	+2.5	0.2–0.4
FB	—	12–14	1.0	+2.5	<0.1

[a] Average oxidation state of the reduced chromium.

H_2-TPR Experiments

The H_2-TPR measurements were performed with an Altamira Instruments AMI-100 catalyst characterisation system. The catalyst samples (30 mg) were flushed with argon and heated from 30 to 115°C at a rate of 11°C/min, and the samples were held at 115°C for 60 min. After that the samples were heated from 115 to 590°C at a rate of 11°C/min under a flow of 5.0% O_2/Ar and kept for 30 min. The samples were cooled to 30°C in 5.0% O_2/Ar flow. TPR was performed at heating rates of 6, 11, and 17°C/min up to 590°C under a flow of 11.2% H_2/Ar (50 cm^3/min). The consumption of hydrogen was monitored with a thermal conductivity detector and recorded at a signal rate of 6 points/min. The hydrogen consumption was quantified by a pulse calibration. The temperature was measured adjacent to the catalyst bed and it followed a strictly linear trend.

In the kinetic modelling of the H_2-TPR patterns, the rate of reduction was unequivocally related to the observed rate of H_2 consumption. Separate mass spectrometer analyses during TPR showed that water was released slightly delayed from the hydrogen consumption and some water was also released later at higher temperatures as a separate process. Retaining a part of the water on the catalyst in H_2-reduction was reported earlier (18). The stoichiometric water release is completed in subsequent oxidation. Thus water production was not considered an appropriate measure of the progress of the reduction.

The selection of experimental conditions was in agreement with the criterion developed by Malet and Caballero (19), $P = \beta S_0/(FC_0) \ll 20$ K (β, heating rate; S_0, initial molar amount of reducible substance; F, volumetric flow rate of reducing agent; and C_0, molar concentration of reducing agent). The instantaneous maximum conversion of hydrogen was less than 6% in our system: thus no hydrogen exhaustion took place. The experimental setup allowed treating the system as a differential reactor. The effect of diffusion of hydrogen in the catalyst pores was considered

in terms of the Weisz–Prater (20) criterion. The value of the criterion ($\ll 1$) indicated that the observed reaction rate was free of the intraparticle mass transfer resistance of the reactant.

Estimation of Kinetic Parameters

Kinetic parameters were estimated using nonlinear regression. The integral equation was numerically solved by either a trapezoidal method or by an adaptive Simpson quadrature, and the object function minimisation was carried out by the Nelder–Mead search method. The criterion for optimisation was the sum of squared residuals (SSR) between the measured hydrogen consumption and the corresponding model output. In the multiresponse fitting, a combined criterion was formed by adding up the SSRs. All the computations were performed in the MATLAB®6 (MathWorks Inc.) environment. The temperature mean-centring was done for the rate coefficients $k(T) = k_{\text{ref}} \exp(E/R(1/T_{\text{ref}} - 1/T))$ in order to enhance parameter identifiability.

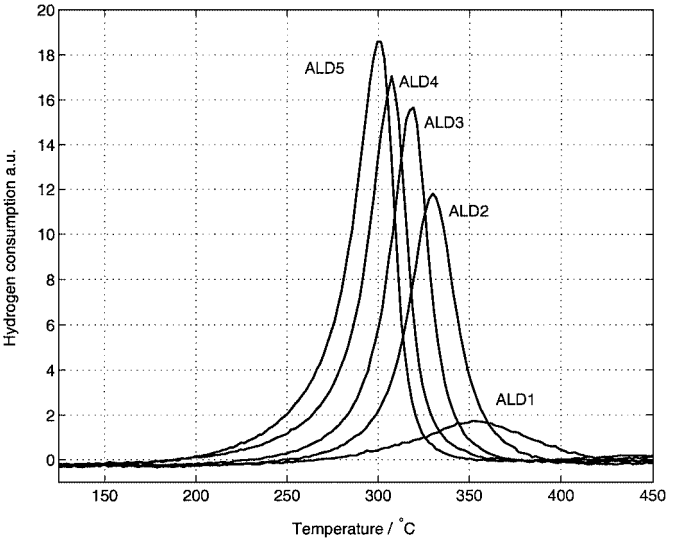

FIG. 2. Measured TPR patterns for ALD samples; heating rate, 11 K/min; reducing agent, 11.2% H_2/Ar at 50 cm^3/min; $m_{\text{cat}} = 30$ mg.

RESULTS

TPR Experiments and the Average Oxidation State of Chromium after Reduction

The H_2-TPR thermograms for the heating rates of 6, 11, and 17 K/min are shown as an example for the ALD5 catalyst in Fig. 1. The reduction rate maxima for the ALD5 catalyst occurred at conversions $\alpha_p = 0.70$, 0.67, and 0.67 and at temperatures $T_p = 555$, 573, and 582 K. The TPR results were typically highly reproducible, with temperatures of rate maxima remaining within ±2 K in repeated runs. The signal quality was good and the detector sensitivity made the quantitative analysis of consumed hydrogen relatively accurate for most samples. The high noise-to-signal ratio in the TPR data of the ALD1 catalyst made that data less accurate than that for ALD2–ALD5.

Figure 2 illustrates the TPR curves of the ALD1–ALD5 samples with a heating rate of 11 K/min. It is seen that the reduction rate maxima shift to higher temperatures as a function of decreasing chromium loading. Figure 3 presents the reduction behaviour of ALD5 together with that of the FB catalyst. As can be seen, reduction of the FB sample starts at substantially a higher temperature than the reduction of ALD5.

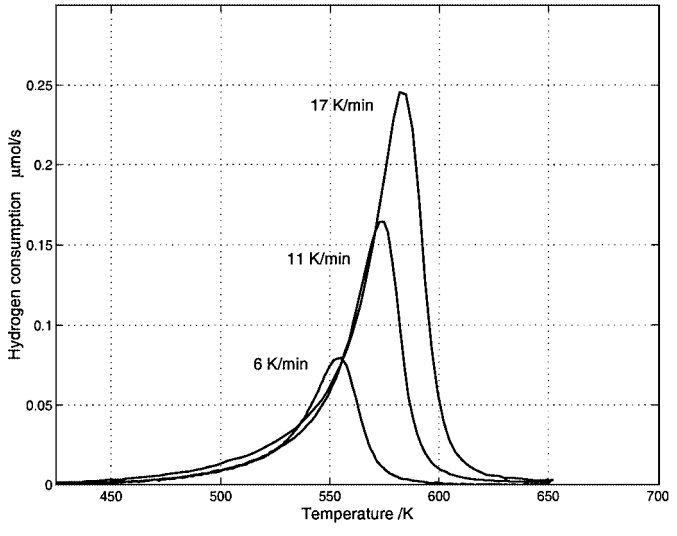

FIG. 1. Measured TPR patterns for the ALD5 catalyst; heating rates 6, 11, and 17 K/min.

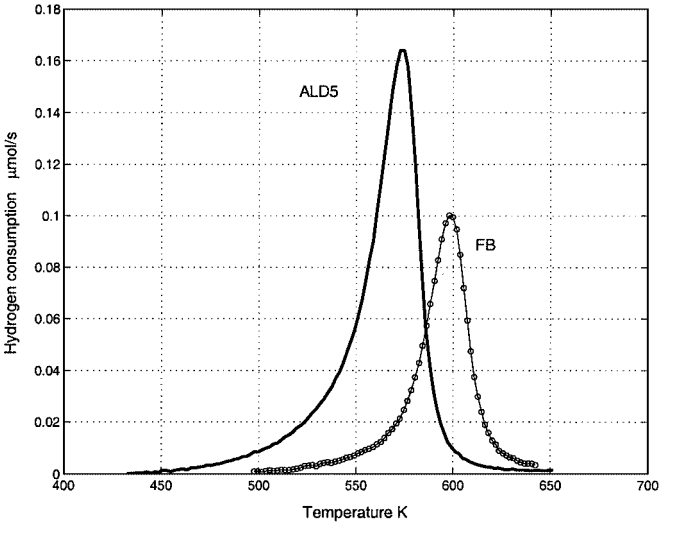

FIG. 3. Measured TPR patterns for ALD5 and FB; heating rate, 11 K/min; reducing agent, 11.2% H_2/Ar at 50 cm^3/min; $m_{\text{cat}} = 50$ mg.

The average oxidation state of the reduced chromium after reduction was calculated from the analysed amount of hexavalent chromium and the consumed hydrogen. The assumed reduction stoichiometry was 1.5 H_2/Cr^{6+}. The hydrogen consumption for each sample was calculated by averaging the consumption values of the repeated runs. The average oxidation states after the reduction are given in Table 1. As can be seen, the average oxidation state for samples ALD1–ALD4 is +3 within experimental error and thus the chromia on these samples follows the presumed reduction stoichiometry. Both samples with high chromium loading (ALD5 and FB) consumed more hydrogen than expected and it is concluded that in part the chromium reduced further than oxidation state Cr^{3+}. The XPS measurements of the reduced ALD5 sample clearly indicated the absence of the peak for Cr^{6+}. XPS also allowed the interpretation that all the chromium after reduction was Cr^{3+}.

Extraction of Apparent Activation Energies of Reduction

The experimental thermograms were analysed using the temperature-programmed Arrhenius plot (the Kissinger method (21)) and the method of constant conversion (the Friedman method (22)). Both these methods require TPR data collected at different heating rates. In the temperature-programmed Arrhenius plot the activation energy estimate (E) is obtained from the shift of the rate maximum temperature (T_m) with heating rate (β). If the plot of $\ln(T_m^2/\beta)$ versus $1/(T_m)$ results in a straight line, the slope of the plot is E/R, where R is gas constant. The conversion at rate maximum is required to be independent of the heating rate. In the method of constant conversion, $\ln(d\alpha/dt)$ is plotted against $1/T$ at selected conversions, and the slope gives $-E/R$. The rate of conversion $d\alpha/dt$ is obtained from the experimental data. Both methods are based on the rate equation of the form

$$\frac{d\alpha}{dt} = k(T)\,f(\alpha)\,f_2\left(C_{H_2}, C_{H_2O}\right), \qquad [1]$$

with

$$\frac{dT}{dt} = \beta. \qquad [2]$$

The rate coefficient $k(T)$ is expressed using the Arrhenius equation $k(T) = A\exp(-E/(RT))$. Function f_2 is assumed to be constant and $f(\alpha)$ is solely a function of the degree of conversion α. The Kissinger peak analysis utilises only the temperatures of the rate maxima, but the method of constant conversion can be applied at different conversion levels to obtain apparent activation energy estimates at different degrees of reduction.

The temperature-programmed Arrhenius plot for sample ALD5 is shown in Fig. 4. Straight lines ($R^2 \sim 0.99$) were obtained for all samples except ALD1 ($R^2 \sim 0.84$) and ALD2 ($R^2 \sim 0.95$). The resulting activation energies for the

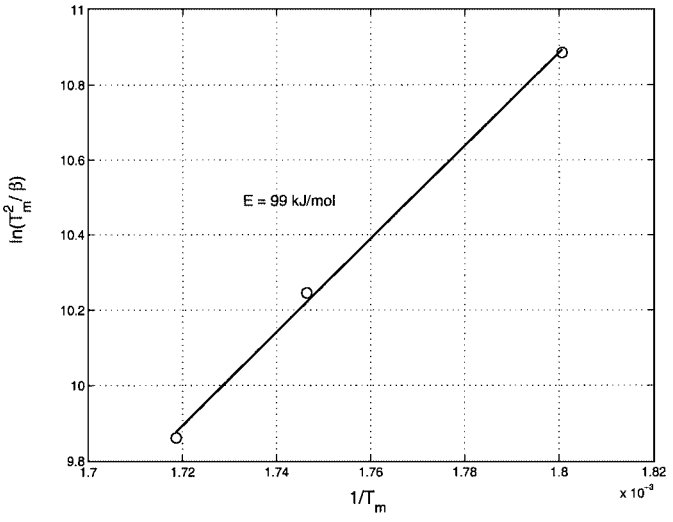

FIG. 4. Temperature-programmed Arrhenius plot for ALD5.

ALD1–ALD5 samples and the FB sample were 111, 85, 87, 96, 99, and 72 kJ/mol, respectively. The plots obtained by the method of constant conversion for the ALD5 catalyst, and the resulting apparent activation energy as a function of reduction degree, $E(\alpha)$, are presented in Figs. 5a and 5b respectively. The trends in $E(\alpha)$ were similar for the samples ALD3–ALD5 and FB: up to $\alpha = 0.5$ the activation energy could be interpreted to be constant, and thereafter there was a steady growth in the value of E. These results are collected in Table 2 for reduction degrees $0 < \alpha < 0.5$ and $0.5 < \alpha < 1$. Samples ALD1 and ALD2 are excluded from Table 2 because the analysis did not yield straight lines. The accuracy of the determined apparent activation energies was roughly within 4 kJ/mol for both methods.

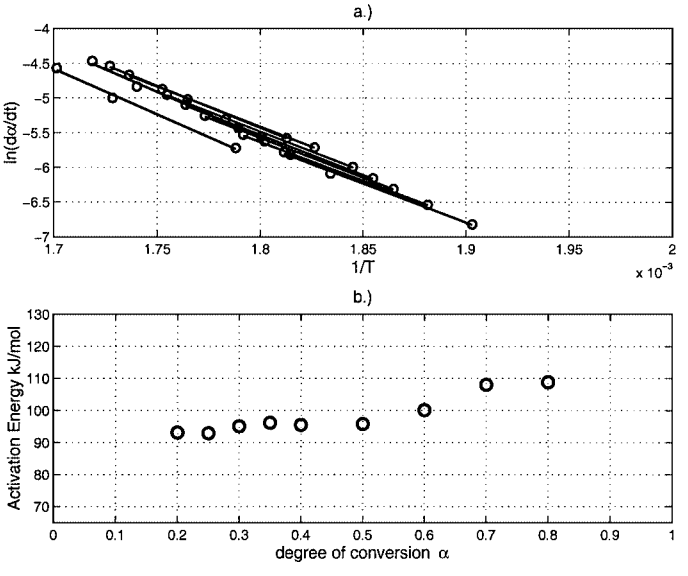

FIG. 5. Method of constant conversion for ALD5. (a) Plots. (b) Apparent activation energy as a function of reduction degree.

TABLE 2

Apparent Activation Energies of Reduction Obtained by the Method of Constant Conversion

Sample	E	
	$0 < \alpha < 0.5$ (kJ/mol)	$0.5 < \alpha < 1$ (kJ/mol)
ALD3	87	87–113
ALD4	98	98–110
ALD5	95	95–108
FB	76	76–99

Kinetic Modelling and Regression Analysis of TPR Data

The experimental data was favourable for more thorough kinetic analysis. Kinetic modelling of the TPR patterns was performed with nonlinear regression analysis. Kinetic models used in this work are collected in Table 3. We previously tested the most common kinetic models for the reduction of the ALD3 catalyst, which we considered the most ideal sample (13). The ALD3 sample was investigated first because its chromium content is close to monolayer coverage. According to Hakuli *et al.* (16), up to monolayer coverage CrO_x is anchored to Al–OH groups in a two-dimensional array, whereas above monolayer content three-dimensional Cr_2O_3 clusters are formed, possibly along with further two-dimensional arrays. We observed that three TPR curves with different heating rates were required to enable discrimination between the five different models. Nucleation and nuclei growth models were found promising and their theoretical foundations were investigated in detail (13). The different forms of nucleation and nuclei growth mechanisms were reconsidered, starting from the work of Avrami (23), and tested for the ALD3 TPR data. The nucleation was modelled to take place as a first-order process with a temperature-dependent rate coefficient, and the growth rate of nuclei was proportional to the rate coefficient of the Arrhenius form as well. The final conclusion of our study (13) was that the reduction kinetics of the ALD3 sample is best described by the two-dimensional nuclei growth model with instantaneous nuclei activation. Nucleation dynamics was not needed to account for the observations. Either there was no time distribution of nucleation events relevant to the time scale of the growth (nuclei were activated to growth almost simultaneously) or the nucleation process just could not be identified on the basis of present data.

Reduction of the other samples (ALD1, ALD2, ALD4, ALD5, and FB) was then investigated. The kinetic parameter estimation was begun using the two-dimensional (2D) nuclei growth model with instantaneous nucleation, the model that was successful in describing the reduction kinetics of ALD3. Three TPR curves for each sample, with heating rates of 6, 11, and 17 K/min, were utilised for model fitting. The reduction kinetics of samples ALD2, ALD4, ALD5, and FB could be explained by the same kinetic

TABLE 3

Kinetic Models of Reduction Applicable for Supported Chromia[a]

Model	Equation
Temperature-dependent first-order nucleation and 2D growth. Nucleation coefficient: $k_2(T) = A_2 \exp(-E_2/(RT))$	$-\ln(1-\alpha(t)) = \int_0^t \left(\int_y^t A \exp\left(-\frac{E}{R(\beta\tau + T_0)}\right) d\tau \right)^2 \left(\frac{dN}{dt}\right)_{t=y} dy,$ where the rate of nucleation is $\left(\frac{dN}{dt}\right)_{t=y} = k_2(y)\, N_0 \exp\left(-\int_0^y k_2(t^*)\, dt^*\right)$
First-order nucleation and 2D growth. Nucleation coefficient: k_2 constant	$-\ln(1-\alpha(t)) = \int_0^t \left(\int_y^t A \exp\left(-\frac{E}{R(\beta\tau + T_0)}\right) d\tau \right)^2 \left(\frac{dN}{dt}\right)_{t=y} dy,$ where the rate of nucleation is $\left(\frac{dN}{dt}\right)_{t=y} = k_2 N_0 e^{-k_2 y}$
Instantaneous nucleation and 2D growth	$-\ln(1-\alpha(t)) = \left(\int_0^t A \exp\left(-\frac{E}{R(\beta\tau + T_0)}\right) d\tau \right)^2$
Random nucleation, i.e., unimolecular decay	$-\ln(1-\alpha(t)) = \int_0^t A \exp\left(-\frac{E}{R(\beta\tau + T_0)}\right) d\tau$

[a] Symbols: α, degree of reduction; t, time; y, nucleation time; A, Arrhenius constant grouped together with other constants; E, activation energy; N_0, number of germ nuclei; β, linear heating rate; and T_0 initial temperature.

TABLE 4

Estimated Kinetic Parameters (2D Nuclei Growth Model) with 95% Confidence Intervals and Root Mean Square Residuals

Sample	E (kJ/mol)	A	rms (μmol/s)
ALD2	81.0 ± 1.0	$(6.6 \pm 1.3) * e4$	3.69e−4
ALD3	98.4 ± 0.8	$(3.5 \pm 0.6) * e6$	3.48e−4
ALD4	94.2 ± 0.8	$(2.4 \pm 0.4) * e6$	3.40e−4
ALD5	84.9 ± 0.9	$(4.1 \pm 0.7) * e5$	3.98e−4
FB	89.0 ± 1.6	$(3.6 \pm 1.1) * e5$	4.45e−4

model as the reduction of the ALD3 sample. The fit of the model to the ALD3, ALD4, and ALD5 data was fairly good; the fit to the ALD2 and FB data was more compromised but adequate. The reduction of ALD1 could not be satisfactorily described by the 2D nuclei growth model. The estimated kinetic parameters with their 95% confidence intervals for ALD2–ALD5 and FB are presented in Table 4. The root mean square errors (rms) between the model and the experimental data are also given as a measure of the goodness of the fit. The best-fit model solution and the experimental data for ALD5 are illustrated in Fig. 6.

After regression analysis using the 2D nuclei growth model with instantaneous nucleation, further modelling was undertaken with the TPR data of ALD1, ALD2, and FB. Among all common kinetic models for reduction, the random nucleation model best described the reduction kinetics of ALD1 catalyst, with kinetic parameters $A = (5.0 \pm 0.6)$e3 and $E = (74.8 \pm 0.6)$ kJ/mol, and rms = 2.15e−5 μmol/s. The fit was not perfect nevertheless. The TPR of the ALD2 catalyst was also challenging: the 2D nuclei growth models did not explain the data totally satisfactorily and the other presently known models were

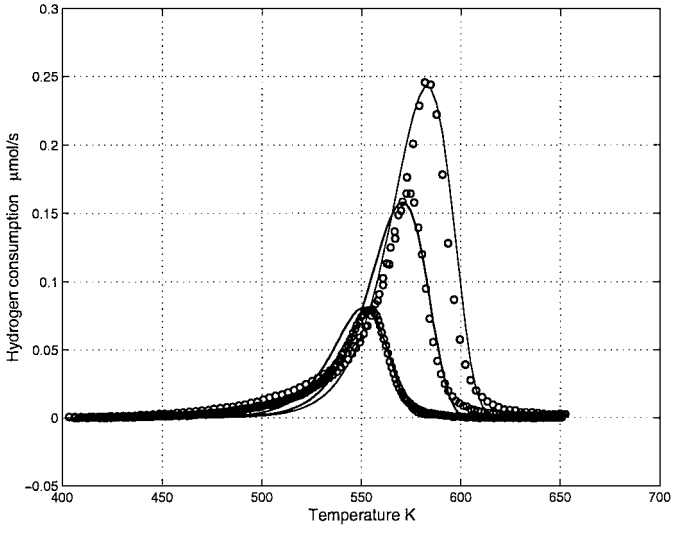

FIG. 6. Kinetic model (—) and TPR data (○) for ALD5 catalyst.

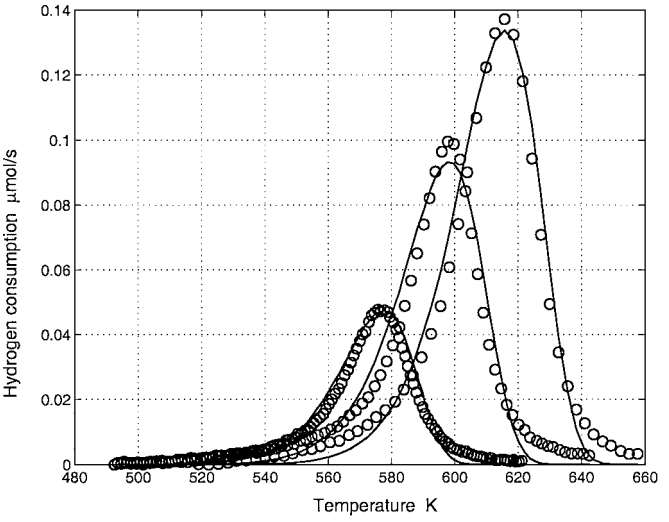

FIG. 7. Kinetic model (—) and TPR data (○) for FB catalyst.

far less successful. As noted above, the reduction of the FB catalyst was fairly well described by the 2D nuclei growth with instantaneous nucleation. The slight deficiency in the fit encouraged further modelling. Application of the full four-parameter form of the nucleation/nuclei growth model resulted in a considerably better fit, but parameter identifiability was seriously deteriorated. The four-parameter model was then simplified by omitting the temperature-dependence of the nucleation rate coefficient. This approach resulted in equally good agreement between the data and the model as provided by the four-parameter model and the parameters were better identified. ($A = (1.8 \pm 0.7)$e4, $E = 78 \pm 2$ kJ/mol, $k_2 = 0.0036 \pm 0.0015$, rms = 2.9e−4 μmol/s). Figure 7 shows the best-fit model solution and the TPR of the FB sample.

DISCUSSION

Qualitative Character of the TPR Patterns

The experimental reduction data clearly exhibited smooth single-peak behaviour. This was the case for all samples examined. Evidently, only one dominant reduction process was taking place and there was no rate-limiting intermediate oxide formation. Single-peak behaviour is surprising, since the chromium oxide species are directly exposed to the heterogeneities of the amorphous support, and the removable oxygen atoms in the chromium oxide could have slightly different reactivities. The diverse nature of the Cr^{6+} species was revealed, for example, in their partial solubility in cold water (16). The good solubility in cold water was attributable to polymeric chromia species with weaker interaction with the alumina support. The solubility of the Cr^{6+} species in cold water increased with loading below monolayer content (25–50% $Cr^{6+}_{sol}/Cr^{6+}_{tot}$) and levelled

off above 7 wt% Cr loading (50% $Cr^{6+}_{sol}/Cr^{6+}_{tot}$). The less soluble Cr^{6+} species were interpreted as grafted, chemically bound to the support. Similar observations have been reported by Cavani *et al.* (24) for impregnated chromia catalysts. Despite the presence of differently bound chromium species, the TPR results indicate that the reducible species are kinetically homogeneous in such a way that their combined reduction behaviour results in a single-peak TPR pattern. The homogeneity of the ALD samples originates in part from the preparation method: the ALD technique ensures the formation of a well-defined surface layer with high lateral dispersion (15). Judging from the regularity of the thermograms, however, the FB catalyst was at least equally homogeneous.

Average Oxidation State of Chromium after Reduction

Comparison of the hydrogen consumption with the amount of Cr^{6+} determined in the calcined sample indicated that hexavalent chromium reduces mainly to the trivalent form (except perhaps for the FB and ALD5 samples). Thus the TPR results agree with the XPS results. The alumina support is known to stabilise the reduction of Cr^{6+} to Cr^{3+}. Samples FB and ALD5, with high chromia loading, appeared to consume more hydrogen than would be expected from the amount of Cr^{6+}. Blank TPR runs with bare alumina ruled out hydrogen-consuming reactions of the support. It may be that high loaded samples reduce partly to Cr^{2+}. The amount of Cr^{6+} species reducible to Cr^{2+} would have to be very low since no such species were detected by XPS. The ALD5 and FB samples might contain microcrystalline or amorphous Cr_2O_3, which might support Cr^{6+} that is reducible to Cr^{2+}. Chromium is known to reduce to oxidation-state Cr^{2+} on silica support where crystalline chromia forms at moderate loadings (25). The Cr^{6+} species on the surface of α-Cr_2O_3 also appear to reduce to oxidation state Cr^{2+} (25).

Apparent Activation Energies of Reduction

The apparent activation energies of reduction obtained using temperature-programmed Arrhenius plots and the method of constant conversion ($0 < \alpha < 0.5$) are in agreement with each other. Since both methods rely on Eqs. [1] and [2] the agreement of the results is expected. If the TPR data is less ideal than in our case, application of more heating rates than three is encouraged. The activation energy values obtained using temperature-programmed Arrhenius plots and the method of constant conversion are not, however, in line with the values obtained using nonlinear regression analysis. Increasing activation energy as a function of α disqualifies the basic assumptions of Eq. [1] and is indicative of convoluted processes. On this basis we propose that complete line-shape analysis of TPR data is a stronger basis for understanding reduction behaviour.

Kinetics of Reduction

The kinetic results allow interpretations regarding the reduction of the ALD samples. Figure 2 shows that the TPR curves of ALD2–ALD5 exhibit similar characteristics, the major trend being the regular shift in the reduction rate maximum to higher temperatures with decreasing chromium loading. The reduction rate regularly increases with loading. The thermogram of ALD1 is distinctly different from the TPR curves of the other ALD samples. In the case of the FB sample (Fig. 3) the TPR pattern does not deviate much from the patterns of the ALD samples, suggesting that the same overall reduction mechanism may be operable. The conducted regression analysis further supports the qualitative observations, since the differences are clearly reflected in the best-fit models. The ALD2–ALD5 and FB samples all follow in some degree the two-dimensional nuclei growth model, whereas the reduction of ALD1 can best be described in terms of random nucleation. We previously interpreted the kinetic results for ALD3 to imply that the reduction reaction does not take place homogeneously all over the surface by random reduction of individual chromia species (13). Instead, nuclei with reduced chromium grow as the reduction proceeds. This mechanism is considered in principle acceptable because chromium oxide has a tendency to form two-dimensional overlayers on alumina, and in this highly dispersed oxide phase the hexavalent chromium is present as surface species. Direct evidence is required to conclusively verify the reduction mechanism of nuclei growth. The nuclei growth mechanism inherently requires that (i) chromium forms relatively big clusters in which the species interact electronically with each other and (ii) the reduction is more favourable at the interface of the old and new phase than in the middle of the old phase. Each and every separate cluster needs to experience nucleation before total conversion takes place; bigger cluster size thus facilitates this topochemical advancement of reduction. In addition, the clustering of chromia might reduce the interaction with alumina and increase the rate of reduction.

The chromium coverage on the alumina support is of interest due to the topochemical models of reduction. In an investigation of the surface coverage of chromia on alumina by ion scattering spectroscopy. Scierca *et al.* (26) found that 2.5 wt% Cr loading resulted in 26% coverage on alumina. Kytökivi *et al.* (15) showed, with low-energy ion scattering (LEIS) measurements, that the intensity of the chromium signal increases linearly with chromium loading up to monolayer content and showed no further increase for a higher loaded sample. Since LEIS probes only the topmost atomic layer it seems probable that below monolayer the coverage is directly proportional to the loading and coverage saturates above monolayer content. This implies that there are uncovered areas of alumina in the present samples and the coverage on ALD2 is about 63% of that on

ALD3. The existing nuclei growth models basically assume that the converting material is contiguous. If the interacting chromia clusters are big enough in relation to nuclei growth rate, the reduction is still adequately described by the nucleation and nuclei growth kinetic model.

It is tempting to interpret the difference between ALD1 and the other ALD catalysts in terms of the lack of topochemistry in ALD1, even though the coordination environment of the chromium species may also be fundamentally different. The relative content of Cr^{6+} in the calcined ALD1 sample is the highest among all the samples. In the preparation of ALD1, monochromates are formed on alumina in a highly dispersed manner due to the saturating, self-terminating reactive adsorption: the steric hindrance of acac ligands does not allow close lateral deposition of chromium species during the first cycle, and the subsequent calcination evidently cannot result in extensive clustering either. These monochromates interact strongly with the support, but very little with each other. The cold-water-soluble Cr^{6+} species on ALD1 was only 25% of the total amount of Cr^{6+} species (16), suggesting a strong interaction of the species with the support. The reduction takes place as a random nucleation of individual monochromates and the separation of the monochromates from one another prevents the topochemical reduction characteristic for higher loaded chromia catalysts.

Poorer quality of the fit of the nuclei growth model with the ALD2 data and parameter values that are barely consistent with those for ALD3–ALD5 suggest that ALD2 is topochemically somewhat different from the higher loaded samples. The chromium content of ALD2 is less than the monolayer content. In ALD2 the chromia presumably does form ensembles in which the species interact electronically with each other. However, the reduction of ALD2 may constitute an intermediate case between genuine nuclei growth (a suitable model for ALD3) and random nucleation (a suitable model for ALD1). The chromia clusters probably reduce by nuclei growth, but the overall nuclei growth model is not completely valid extent because the chromium oxide clusters are not big enough or the cluster size distribution varies too widely. The reduction of numerous small clusters becomes rate limiting and the existing kinetic model does not include a mechanism for accounting for the CrO_x cluster size distribution.

Loading close to or beyond the monolayer content (ALD3–ALD5, FB) further increases the interchromia interactions and the nuclei growth mechanism becomes properly operable. The 2D nuclei growth model describes the experimental data well. Monolayer content does not mean 100% coverage on alumina (15) but rather is a threshold for the formation of a three-dimensional oxide phase. The amount of Cr^{6+} stabilises above the monolayer content. In addition, according to Hakuli *et al.* (16) the cold-water-soluble fraction of Cr^{6+} is constant, implying that certain polymeric species are equally abundant in ALD3–ALD5. Thus the main difference is that less of the Cr^{6+} species is in direct contact with the support in ALD4 and ALD5 than in ALD3. The removable oxygen atoms attached to the chromia species formed on chromium oxide exist in a different environment than the removable oxygen atoms in monolayer coverage. The reactivity in the "second layer" is slightly higher. In kinetic modelling this is reflected in the best-fit rate parameters: the activation energy of nuclei growth decreases with increasing loading from ALD3 to ALD5. This increase in growth rate with loading is partly compensated for by the decreasing preexponential factor.

As shown by the TPR data of the FB and ALD5 samples in Fig. 3, the reduction starts at a substantially higher temperature for FB. On the other hand, if we look at the temperature range of the complete reduction process (the temperature window), the FB catalyst is reduced in a temperature window narrower than that of all the other samples, which suggests greater homogeneity of the reducible species. The higher starting temperature might also be due to homogeneity and to a smaller number of defects available to act as germ nuclei. The FB and ALD samples contain comparable amounts of total chromium, but the Cr^{6+} contents are very different. There was also a difference in stability in five successive calcination–TPR cycles, as shown by Airaksinen *et al.* (27). The reduction rate maximum of the ALD5 catalyst shifted to higher temperatures, whereas the reduction rate maximum of the FB catalyst remained the same during five TPR runs. Furthermore, the five H_2-TPR curves showed a faster decrease in the amount of Cr^{6+} for ALD catalyst. These observations imply certain structural differences between the ALD5 and FB catalysts. Perhaps, in repeated runs, the topochemistry of ALD5 changes with decreasing dispersion, and chromia accumulates at anchoring points on the support. The differences in reduction behaviour between ALD and FB samples could be support-induced and related to the preparation techniques.

We now turn our attention to the kinetic models of reduction applicable for the ALD3–ALD5 and FB catalysts. The overall mechanism featured is the 2D nuclei growth mode. In addition to this similarity, there is a clear difference between the ALD5 and the FB samples: the reduction of the FB sample is better described by the model with non-instantaneous nucleation. If we compare the estimates for the two-parameter model for the ALD5 and FB samples, we find that the preexponential factors are comparable although the activation energy of nuclei growth is higher for the FB catalyst. The reduction kinetics of the FB catalyst is, nevertheless, considerably better described by the model in which the nucleation is a dynamic process in its own right (the three-parameter model). The estimated rate constants of the three-parameter model imply somewhat difficult nucleation and relatively easy subsequent nuclei

growth. Either the parameter estimation for the FB catalyst adventitiously benefited from the increased degrees of freedom, or else the reduction mechanism really involved two rate-limiting processes. Implications of these kinetic modelling results are in accordance with the qualitative observations of the TPR pattern: reducible chromium appears be more homogeneous on the FB sample than on the ALD5 sample.

The general applicability of the two-dimensional nuclei growth model is probably confined to the reduction of supported oxide systems where the oxide material has a tendency to form relatively large monolayer clusters. The amount of dispersed oxide on the support is of significance, as was shown in this study. Samples which do not reduce according to the nuclei growth model probably carry scattered chromia species in weak interaction with each other. Thus TPR kinetic modelling provides information on the mode of organisation of the reducible species on the catalyst support.

CONCLUSIONS

Kinetics of the reduction of six chromium oxide catalysts (total chromium content, 1.2–14 wt%) was studied using nonlinear regression analysis. Satisfactory kinetic modelling was accomplished for all samples. The nuclei growth reduction model very well described the reduction behaviour of the alumina-supported chromium oxide catalyst when the chromium loading was close to or greater than the monolayer content. This was the case for samples ALD3–ALD5 and the commercial fluidised bed catalyst. The sample with low chromium content (ALD1, 1.2 wt%) seemed to reduce using a different overall mechanism. The intermediate loaded samples (4–5 wt%) probably reduce by nuclei growth, but the applicability of the nuclei growth model requires that the size of the chromia clusters not be too small. Total chromium content affects reduction behaviour through a topochemical mechanism. This, again, underlines the importance of studying higher loaded samples when the behaviour and structure of real working catalysts need to be understood. Complete line-shape analysis of TPR patterns offers a means for quantitative characterisation of alumina-supported chromium oxide catalysts.

ACKNOWLEDGMENTS

The Academy of Finland is gratefully acknowledged for financial support. Dr. A. Kytökivi is thanked for the preparation of the catalysts, Ms. N. Tyynelä for experimental work, and Mr. K. Kanervo for mathematical consultation.

REFERENCES

1. Weckhuysen, B. M., Wachs I. E., and Schoonheydt, R. A., *Chem. Rev.* **96**, 3327 (1996).
2. Ehrhardt, K., Richter, M., Roost, U., and Öhlmann, G., *Appl. Catal.* **17**, 23 (1985).
3. Fouad, N. E., Knözinger, H., and Zaki, M. I., *Z. Phys. Chem.* **186**, 231 (1994).
4. Mentasty, L. R., Gorriz, O. F., and Cadus, L. E., *Ind. Eng. Chem. Res.* **40**, 136 (2001).
5. Hurst, N. W., Gentry, S. J., Jones, A., and McNicol, B. D., *Catal. Rev.–Sci. Eng.* **24**, 233 (1982).
6. Jones, A., and McNicol, B. D., "Temperature-Programmed Reduction for Solid Materials Characterization," Dekker, New York, 1986.
7. Knözinger, H., *in* "Handbook of Heterogeneous Catalysis" (G. Ertl, H. Knözinger, and J. Weitkamp, Eds.), Vol. 2, p. 676. VHC, Weinheim, 1997.
8. Monti, D. A. M., and Baiker, A., *J. Catal.* **83**, 323 (1983).
9. Malet, P., and Caballero, A., *J. Chem. Soc. Faraday Trans.* **84**, 2369 (1988).
10. Tarfaoui, A., Ph.D. thesis. Technische Universiteit Delft, The Netherlands, 1996.
11. Dekker, F. H. M., Klopper, G., Bliek, A., Kapteijn, F., and Moulijn, J. A., *Chem. Eng. Sci.* **24A**, 4375 (1995).
12. Bensalem, A., Weckhuysen, B. M., and Schoonheydt, R. A., *J. Phys. Chem. B* **101**, 2824 (1997).
13. Kanervo, J. M., and Krause, A. O. I., *J. Phys. Chem. B* **105**, 9778 (2001).
14. Hakuli, A., and Kytökivi, A., *Phys. Chem. Chem. Phys.* **1**, 1607 (1999).
15. Kytökivi, A., Jacobs, J. P., Hakuli, A., Meriläinen, J., and Brongersma, H. H., *J. Catal.* **162**, 190 (1996).
16. Hakuli, A., Kytökivi, A., and Krause, A. O. I., *Appl. Catal. A* **190**, 219 (2000).
17. Haukka, S., and Saastamoinen, A., *Analyst* **117**, 1381 (1992).
18. Hakuli, A., Kytökivi, A., Krause, A. O. I., and Suntola, T., *J. Catal.* **161**, 393 (1996).
19. Malet, P., and Caballero, A., *J. Chem. Soc. Faraday Trans.* **84**, 2369 (1988).
20. Fogler, H. S., *in* "Elements of Chemical Reaction Engineering," 3rd ed. p. 758. Prentice Hall, Englewood Cliffs, NJ, 1999.
21. Kissinger, H. E., *Anal. Chem.* **29**, 1702 (1957).
22. Friedman, H. L., *Polym. Sci. C* **6**, 183 (1965).
23. Avrami, M., *J. Chem. Phys.* **7**, 1103 (1939).
24. Cavani, F., Koutyrev, M., Trifiro, F., Bartolini, A., Ghisletti, D., Iezzi, R., Santucci, A., and Del Piero, G., *J. Catal.* **158**, 236 (1996).
25. Hakuli, A., Harlin, M. E., Backman, L. B., and Krause, A. O. I., *J. Catal.* **184**, 349 (1999).
26. Scierca, S. J., Houalla, M., Proctor, A., and Hercules, D. M., *J. Phys. Chem. B* **99**, 1537 (1995).
27. Airaksinen, S. M. K., Kanervo, J. M., and Krause, A. O. I., *Stud. Surf. Sci. Catal.* **136**, 153 (2001).